



Active entanglement enables stochastic, topological grasping

Kaitlyn Becker^{a,b}, Clark Teeple^a, Nicholas Charles^a, Yeonsu Jung^a, Daniel Baum^c, James C. Weaver^{a,d}, L. Mahadevan^{a,e,f,1}, and Robert Wood^{a,1}

Edited by Yihui Zhang, Tsinghua University, Beijing, China; received June 7, 2022; accepted September 12, 2022 by Editorial Board Member Yonggang Huang

Grasping, in both biological and engineered mechanisms, can be highly sensitive to the gripper and object morphology, as well as perception and motion planning. Here, we circumvent the need for feedback or precise planning by using an array of fluidically actuated slender hollow elastomeric filaments to actively entangle with objects that vary in geometric and topological complexity. The resulting stochastic interactions enable a unique soft and conformable grasping strategy across a range of target objects that vary in size, weight, and shape. We experimentally evaluate the grasping performance of our strategy and use a computational framework for the collective mechanics of flexible filaments in contact with complex objects to explain our findings. Overall, our study highlights how active collective entanglement of a filament array via an uncontrolled, spatially distributed scheme provides options for soft, adaptable grasping.

entanglement | filaments | soft robots | soft robotic grasping | soft actuators

Securely grasping an object typically requires some knowledge of its size, shape, and mechanical properties. In the natural world, this is done, seemingly without effort, by elephants, whose trunks can pick up a peanut or uproot a tree; orangutans, whose combination of reaching and grasping allows them to swing effortlessly through tree branches; or a jellyfish, whose tentacles collect stunned prey (1-3). In the engineered world of robotic grasping, much work has focused on understanding how to design the mechanics and dynamics of gripper hardware, as well as how to control such devices to interact with objects in the desired way. The form and stiffness of the grasper (relative to that of the target) determines the number (topology), shape (geometry), and magnitude (mechanics) of contacts and associated stresses on target objects (4, 5). The majority of general-purpose graspers, inspired primarily by the remarkable dexterity of the human (and primate) hand, take the form of an articulated set of rigid links that are controlled locally, while a visual-motor feedback loop links perception, planning, sensing, and grasping actions (6, 7).

Modern rigid grippers show great promise, with many controllable degrees of freedom and embedded sensors (8–11), but can present challenges for grasp planning and control in the presence of uncertainty or with complex target geometries (12, 13). One widely explored solution is to employ machine-learning techniques to train grasp-planning algorithms on large, diverse object sets (14, 15). However, learning approaches typically require huge amounts of data, and results are notoriously difficult to generalize. The incorporation of sensory feedback via sophisticated sensing and compliant contact surfaces is another approach that helps rigid robots adapt to target objects with challenging geometries and mechanics (16, 17). Furthermore, adding strategic compliant elements into otherwise rigid fingers obviates the need for explicit sensing and provides a form of mechanical intelligence that drastically reduces the planning and control requirements for successful grasping (18–21).

An alternate strategy for robotic grasping is the use of soft actuators that avoid computational feedback control and, instead, rely on mechanical deformation at multiple scales, both proximally and distally. Extending the concept of strategic compliance, soft grippers and hands devolve some of the mechanical complexity of a grasping task into morphology and passive mechanics of the gripper structure (22). This approach leads to conformable contact that, even in the absence of feedback control, is adaptable and robust to a range of variations in the target shape, size, and properties and robust to damage in the hardware itself (23, 24). While many soft robotic grippers are constructed by using a hand-centric design paradigm, where several digits are attached to a central hub (25–27), soft materials lend themselves well to more interesting and useful shapes and forms via particle jamming (28), origami (29, 30), and other means (24). The multiscale softness of these grippers' surfaces can thus participate in a range of contact configurations with the target, even with relatively simple control. Similarly, continuum actuators in such examples as robotic tentacles (31–36), snakes (37), and plant tendrils and their mimics (38, 39) leverage flexibility to adapt to a range of target objects; an extreme example is that of a colony of worms that can entangle/disentangle to environmental stimuli (40).

Significance

How might one design a grasping system that can handle the topological complexities of branched soft objects? Here, we introduce the notion of entanglement grasping, a nondeterministic approach that circumvents challenges of object recognition, grasp planning, and feedback, via a randomly distributed array of contacts via filament-like soft actuators. Each highly compliant filament has the capacity to conform locally with a target object; the combination of filament-object and filament-filament interactions contribute to a grasp that can be greater than the sum of its parts and provides schemes for soft, adaptable grasping.

Author affiliations: aSchool of Engineering and Applied Sciences, Harvard University, Cambridge, MA 02138; ^bDepartment of Mechanical Engineering, Massachusetts Institute of Technology Cambridge, MA 02139; Department of Visual and Data-Centric Computing, Zuse Institute Berlin, 14195 Berlin, Germany; dWyss Institute for Biologically Inspired Engineering, Harvard University Cambridge, MA 02138; Department of Physics, Harvard University Cambridge, MA 02138; and Department Organismic and Evolutionary Biology, Harvard University Cambridge, MA 02138

Author contributions: K.B., C.T., N.C., L.M., and R.W. designed research; K.B., C.T., N.C., Y.J., and J.C.W. performed research; K.B., C.T., N.C., Y.J., D.B., J.W., L.M., and R.W. analyzed data; and K.B., C.T., N.C., Y.J., D.B., L.M., and R.W. wrote the paper.

The authors declare no competing interest.

This article is a PNAS Direct Submission. Y.Z. is a guest editor invited by the Editorial Board.

Copyright © 2022 the Author(s). Published by PNAS. This article is distributed under Creative Commons Attribution-NonCommercial-NoDerivatives License 4.0 (CC BY-NC-ND).

¹To whom correspondence may be addressed. Email: rjwood@g.harvard.edu or lmahadev@g.harvard.edu.

This article contains supporting information online at https://www.pnas.org/lookup/suppl/doi:10.1073/pnas. 2209819119/-/DCSupplemental.

Published October 10, 2022

These naturally occurring biological examples raise the question of how to engineer a grasping strategy for objects that are geometrically and topologically complex, and perhaps mechanically heterogeneous-e.g., porous or branched structures, such as a small potted plant or a fragile marine coral. Here, we move away from previous works with soft continuum actuators/tentacles in the purposeful use of arrays of long and slender actuated filaments to achieve stochastic topological grasping using filament-target and filament-filament entanglement. By engineering an array of pneumatically actuated filaments on the size scale of desired target objects, we realize a grasping strategy capable of adapting to the topological, geometric, and mechanical complexity of a range of target objects with minimal planning and no perception or feedback control. The basic building block of this strategy, shown in Fig. 1 A and B, is a slender elastomeric filament, whose curvature can be modulated via pneumatic actuation. To become entangled and adapt to different grasping configurations, filaments must achieve sufficient curvature to bend and coil around each other and the target object, made possible by their slenderness. Coiling of our filaments is actuated via inflation of an off-center axial channel, which is sealed at one end. When an individual filament is actuated, it bends because of the eccentricity of the wall thickness, as shown in Fig. 1B. This design enables the filament to deform into a highly curved state to form soft distributed contact zones, either with a target object, itself, or other filaments as it reaches its operational pressure, as shown in Fig. 1C. The filaments were made following a dip-coating technique (41), complementing a recently proposed alternative molding method (42), that allows the characteristic filament curvature to be controlled by the position of the axial channel, and their operating pressure can be tuned by the wall thickness. Dipcoating methods (see SI Appendix, SI Text for details) allow for cheap, easy, and uniform construction of large arrays of actuators with a high aspect ratio (exceeding 200:1), while bubble casting allows for greater variation in the filament geometry before and after actuation. Both methods achieve filaments with large aspect ratios, which would be difficult to construct via other methods, allowing for soft entanglement.

When combining filaments into arrays for grasping, a variety of design parameters can be chosen, depending on the application requirements. For demonstration purposes, the configuration shown in Fig. 1A and used in the experiments below uses 12 300mm-long filaments connected to a single pressure source. Eight of the filaments are distributed evenly around a 50-mm-diameter circle, and four of the filaments are evenly distributed around a 25-mm-diameter concentric circle (see SI Appendix, SI Text for further details). Not all of the 12 filaments will engage directly with an object for every grasp, as shown in Fig. 1D, but the array can also be modified to incorporate more filaments (or a higher density of filaments) and increase the chance of entanglement. To demonstrate the topological complexity of structures for which we can achieve active collective entanglement using this approach, Fig. 1E shows how, through filament self-entanglement, it is possible to cradle a spherical tennis ball, a bar clamp, and a branched tree [the latter of which is typically quite challenging for traditional grippers (13)]. This soft adaptation, which occurs without perception, planning, or feedback, is due to the geometrically and topologically driven compliance of the actuated filament array as it interacts with complex objects.

To quantify entanglement, we adapt ideas from knot theory and consider mesoscopic spherical volumes shown in Fig. 2A that are larger than filament radii and smaller than the filament length and overall gripper dimensions. Within these volumes, we introduce the average crossing number (ACN), defined as the average number of (unsigned) crossings of a filamentary structure over all possible viewing angles. The ACN provides an upper bound on the true (knot theoretic) topological complexity of filaments (43), so that we are guaranteed a conservative estimate of entanglement. Using the notation $e_{\alpha\beta}$ for the ACN between two open curves, $\alpha: I \to \mathbb{R}^3$ and $\beta: J \to \mathbb{R}^3$, we write:

$$e_{\alpha\beta} = \frac{1}{2\pi} \iint_{I \times J} \frac{|(\mathbf{dr}_i \times \mathbf{dr}_j) \cdot (\mathbf{r}_i - \mathbf{r}_j)|}{|\mathbf{r}_i - \mathbf{r}_j|^3}, \quad [1]$$

where \mathbf{r}_i , \mathbf{r}_j are the positions, and $d\mathbf{r}_i$, $d\mathbf{r}_j$ denote the infinitesimal tangent vectors along the centerline of α and β , respectively. For a pair of filaments, the ACN will be smallest when the two filaments are parallel and/or the filaments are far apart from each other, consistent with our intuition that such filament pairs are not entangled. By choosing a mesoscopic volume over which to evaluate the ACN that is larger than the filament radius, but smaller than the system size, we can construct a scalar metric that provides a quantitative measure of entanglement.

We use the actuated filament-object configuration obtained with a computed tomography (CT) scanner to deploy these metrics. In Fig. 2C, we show the segmented and reconstructed scans of a set of structures (using the commercial software Amira) in increasing order of relative entanglement. The objects in Fig. 2C correspond to those shown in Fig. 1E, though the grasp is different, and individual filaments are colorized for easier visualization. The filament center lines were used to compute the local spatial density of filaments, the local ACN, and the ACN of the entangled filament array within a 20-mm-radius spherical volume, as described above. In Fig. 2D, we show the spatial density, and in Fig. 2E, we show the local ACN (see SI Appendix, SI Text for further details). In Fig. 2*F*, we show the contacts between the object and a filament colored in red and contacts between filaments colored in blue (see SI Appendix, Fig. S6 for magnified views). As expected from the adaptive qualities of the filaments, the spatial organization of object contacts and interfilament contacts changes with the topology of the target object. As compared to the simple sphere (tennis ball), the boundaries of the bar clamp and eight-branch tree grasps become more complex and represent a qualitative departure from traditional grasping (4). By applying the same 20-mm-radius bounding sphere from the filament destiny and local entanglement metrics in Fig. 2 C and D, we can compare the probability density of the filament-filament contacts with the local entanglement for each of the four grasps, as shown in Fig. 2G. There is a high similarity between the entanglement and contact distribution, as well as between the four representative objects. Further analysis in SI Appendix, Fig. S7-S9 shows the effect of object shape on the spatial distribution of the contact points, as well as the effect of object shape on the area of contacts.

In general, the ACN between an object and the filaments cannot be defined because objects like a sphere cannot be represented by parameterized curves. However, a slender object like the eightbranch tree can be parameterized by a curve in space; thus, the ACN between the object and surrounding filaments can be calculated by using Eq. 1. The total ACNs of the filaments (averaged over two micro-CT-scanned instances for each object) for each of the four cases in Fig. 2 are similar: 14.5 for the filaments without an object, 14.3 for a tennis ball, 14.5 for the bar clamp, and 14.9 for the test tree. If the branches of the test tree are considered in the ACN, however, the value increases to 22.4, suggesting that an object itself can contribute to the quality of collective entanglement for a more robust grasp. An area of future work to more fully explore and utilize entanglement grasping would be to extend the quantification methods for characterization of

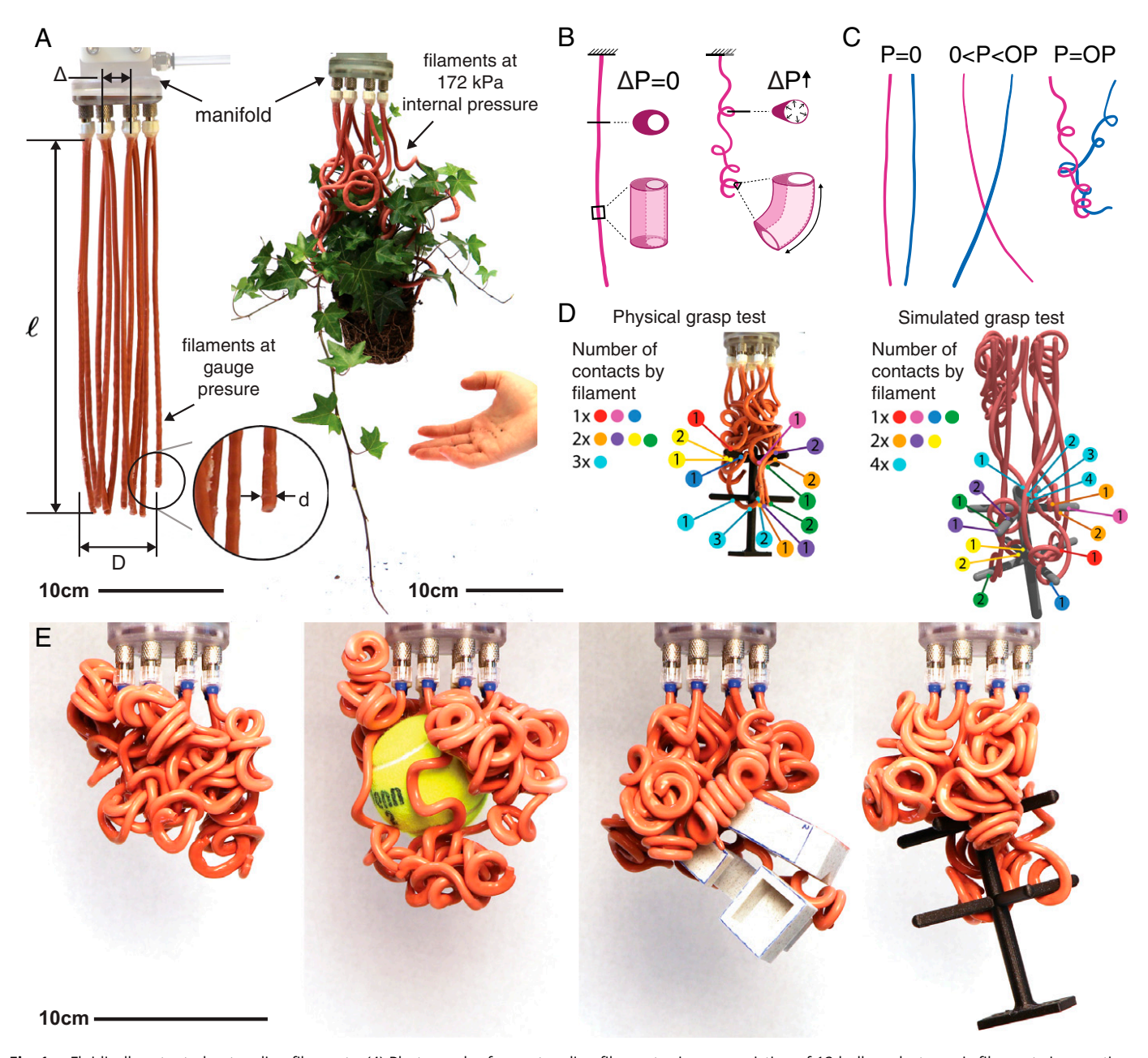


Fig. 1. Fluidically actuated entangling filaments. (A) Photograph of an entangling filament gripper consisting of 12 hollow elastomeric filaments in a resting state and pneumatically actuated around a house plant. (B) Schematic of filaments at ambient and increased internal pressure. (C) Schematic of the entanglement of two nearby filaments. The filaments are not entangled in their rest state or at low pressures. At low pressures, the filament begins to curl in a plane, and as the internal pressure approaches the operating pressure (in this case 172 kPa), the filaments bend out of their initial plane and start to entangle with nearby filaments. (D) Physical and simulated entanglement examples with contacts between filaments and the object (eight-branch tree) indicated. Contacts are color-coded and grouped by individual filaments. (E) Photographs of an array of 12 filaments activated by an internal pressure of 172 kPa and entangled around neighboring filaments and various objects.

nonslender objects. From the scans shown in Fig. 2, however, we can qualitatively say that the object entanglement increases from the sphere, to the bar clamp, to the eight-branch tree.

Collective entanglement of soft individual filaments eliminates the need for fine-grained planning and perception prior to grasping by distributing soft contacts across multiple filaments for greater cumulative engagement and entanglement with other filaments, the target object, or a combination of both. This strategy works particularly well in situations that are challenging for traditional soft and rigid grasping strategies—e.g., in grasping of topologically complex and delicate structures, where traditional grasping notion of force closure used in deterministic grasping (6, 44) is difficult to apply, owing to the variability of contact number, size, and shape and the corresponding contact forces.

In order to compare entanglement-based grasping of target objects with more deterministic approaches, we use two experimental approaches, measuring the entanglement forces and grasp toughness and measuring the grasp success when subject to positioning offsets (see SI Appendix, SI Text for more details of the methods). We define entanglement toughness as the energy required to pull an object out of the grasp and measure it using our 12-filament platform by attaching an object rigidly to the frame of an Instron universal testing machine and measuring the force-displacement curve until failure (see SI Appendix, Fig. S4 for an image of the setup and details). For an operating pressure of 172 kPa (25 psi), we find that the maximum grasping forces achieved over the various objects was 27.6 N, which is comparable to many robotic hands with soft, pneumatic fingers operating

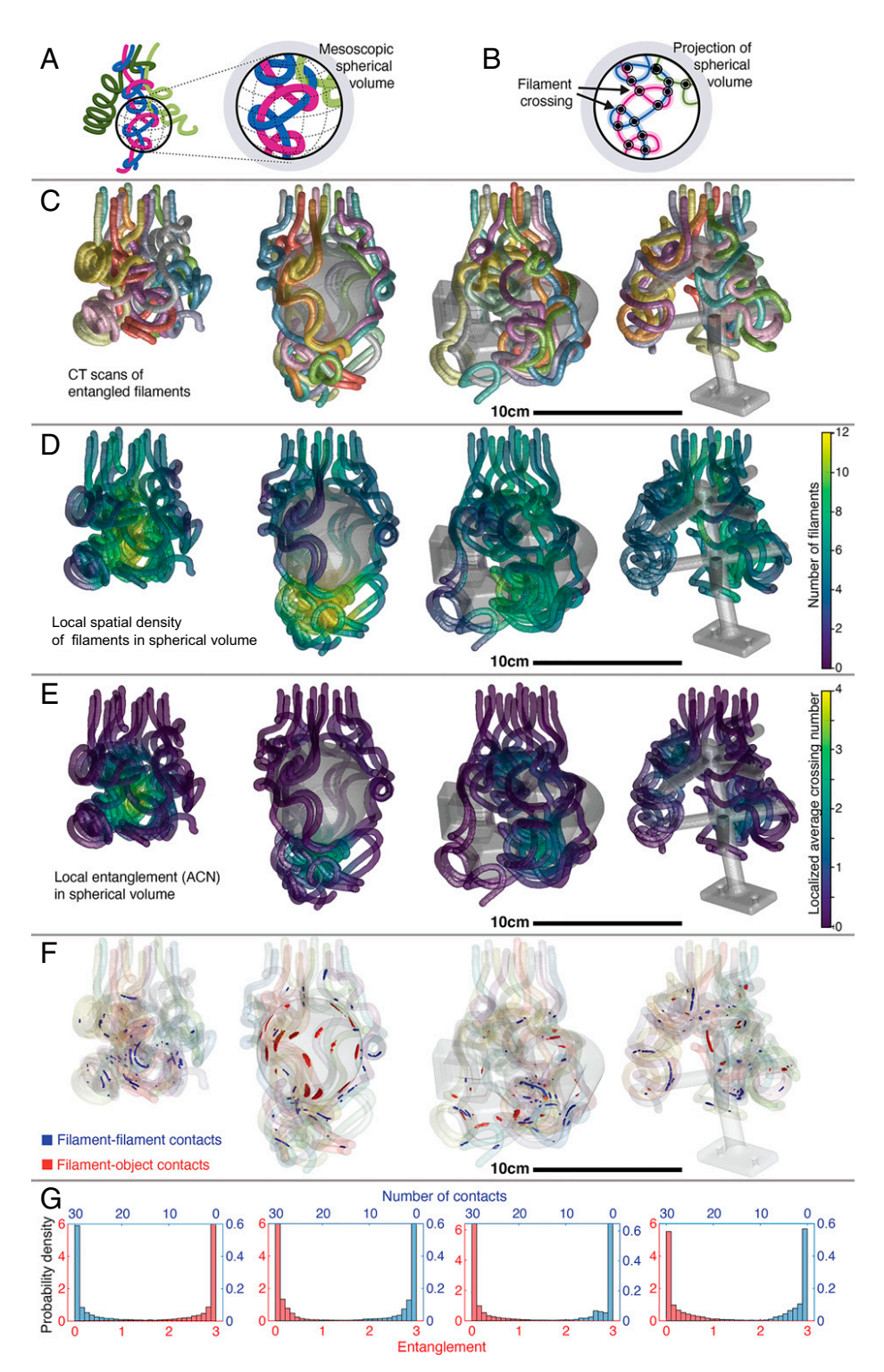


Fig. 2. Spatial distribution of contacts and entanglement. (A) Schematic of four entangled filaments and a spherical bounding volume used to isolate and evaluate local metrics, such as the spatial density of filaments and the localized entanglement density, the results of which are presented in D and E. (B) The spherical bounding volume is projected onto a plane, and the number of crossings between filament center lines is used as an indicator of entanglement. The average over all projection directions is used to find an ACN. (C) Micro-CT-based three-dimensional (3D) reconstructions of the entangled filaments and objects used to extract the position and shape of each filament. Each filament is uniquely colored to distinguish individuals among the given 12-filament array. (D) Spatial density of filaments, calculated based on the number of filaments that occur within a spherical bounding volume with a 20-mm radius. The colors correspond to the number of filaments inside the local bounding volume. (E) Localized ACN of the filaments, calculated as an average number of filament crossings over all projections of a spherical bounding volume with a 20-mm radius. The colors correspond to the ACN within the local bounding volume. (F) A 3D rendering from micro-CT scans of entangled filaments, with filament-filament contacts highlighted in blue and filament-object contacts highlighted in red. The entanglement examples and objects are the same as those shown in Fig. 1E and panels C-E of this figure. (G) Plots of the probability density of the entanglement number (red) and number of contacts (blue) in a 20-mm-radius spherical bounding volume at each point of the array from the scanned grasps shown in C-F. Additional plots for spatial distribution and area of contact are included in SI Appendix, Fig. S7-S9.

at similar pressures (24). Toughness values for the entangling 12-filament gripper range from 10 mJ for a 10-cm sphere, to 380 mJ for a simple branched structure, and 770 mJ for a

vertical 51-mm cylinder, consistent with our intuition that increasing object complexity (for the branched structure) and contact area (for the cylinder) increases the entanglement toughness.

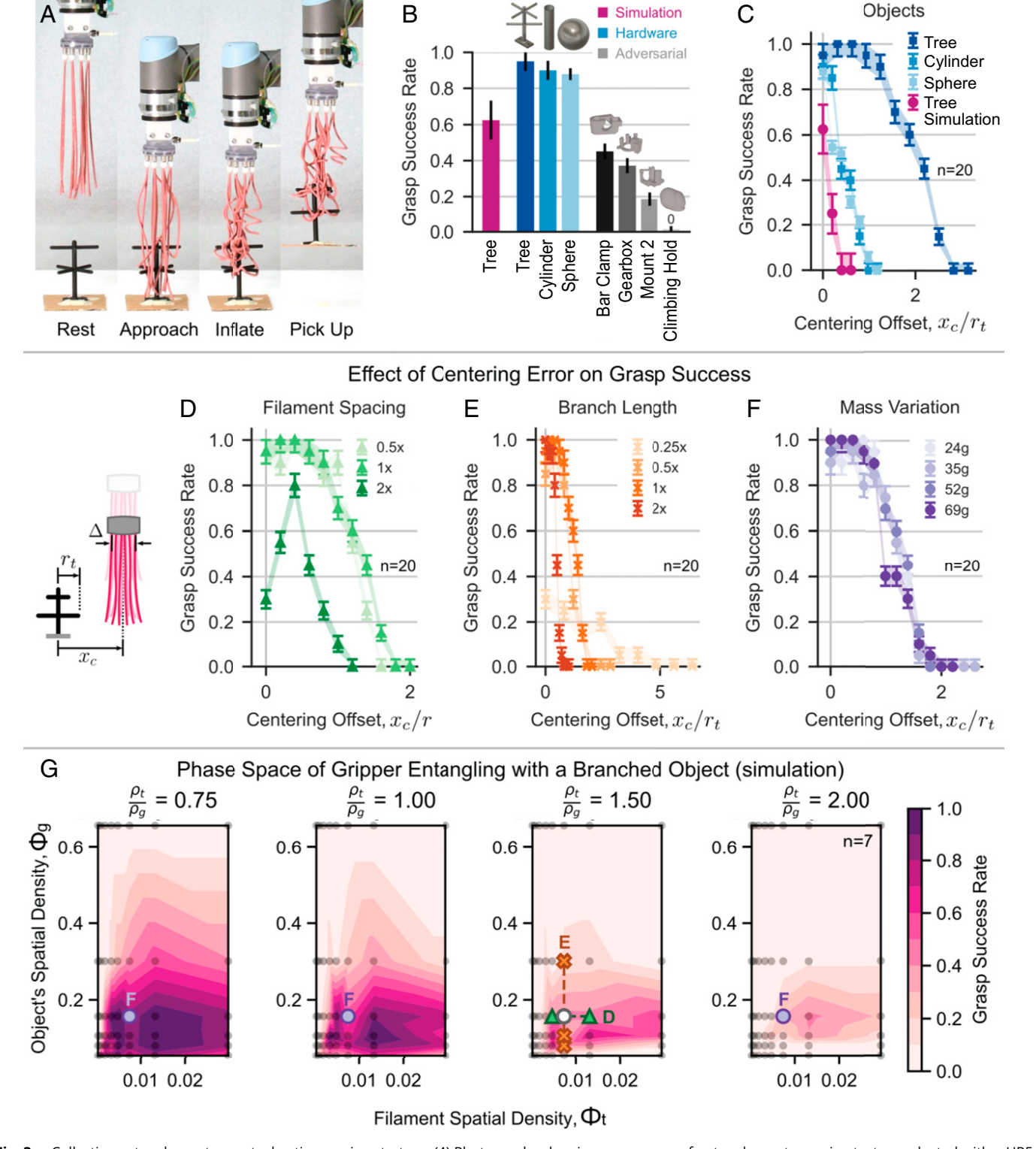


Fig. 3. Collective entanglement as a stochastic grasping strategy. (A) Photographs showing a sequence of entanglement grasping tests conducted with a UR5 robotic arm. (B) Success rate of grasping tests performed with various objects that were centered directly below an array of 12 filaments. Objects include the eight-branch tree shown in B, a 38-mm-diameter cylinder, a 10-cm-diameter sphere, and four objects from an adversarial object set (12). Additional object information is included in SI Appendix, SI Text. All simulated tests were performed with the eight-branch tree. (C) Success rate of a grasping test performed with various objects with increasing horizontal offsets between the vertical center line of the array of filaments and the target object. (D) Grasping-test success rates for a branched object with varying filament spacing and increasing horizontal offsets. (E) Grasping-test success rates for a branched object with varying spatial density (branch length) and increasing horizontal offsets. (F) Grasping-test success rates for a branched object with four different weights and increasing horizontal offsets. (G) Phase space of grasp success rate predicted by simulations of filaments entangling with the branched test object. Each plot represents a different object weight. Sweeps of object spatial density and filament spatial density are shown within each plot. The phase-space locations corresponding to data in D, E, and F are indicated on the plots.

For comparison, values for the grasp toughness of recently developed soft grippers holding onto cylinders with diameters of 51 to 76 mm are 200 to 700 mJ (see SI Appendix, SI Text for details).

To evaluate the efficacy of entanglement in successfully grasping, lifting, and moving an object from its initial to its final position, we used sequences like those shown in Fig. 3A with a sphere, a hollow cylinder, and four objects identified as part of an adversarial object set for robotic grasping (12) (see SI Appendix, Fig. S2 for details on test objects). The approach trajectory in all cases consisted of draping the filament array over the target object from above ("top-drape") by using a robot arm (UR5e, Universal Robots) with 20 grasp trials per object, the results of which are shown in Fig. 3B. We evaluated the entanglement gripper's sensitivity to positioning errors using grasps with controlled centering offsets in increments of 10 mm for 20 trials at each location. (See SI Appendix, and Movie S1 for further testing information.) The results of these experiments are shown in Fig. 3C as a function of the offset between the center axis of the gripper and the center axis of the target object (normalized to the object radius). We found that the entanglement gripper is tolerant to large centering errors (grasp success diminishes by less than 10% for centering errors of 0.2× the object's radius or less) and particularly large errors for the eight-branch tree (less than 10% reduction in grasp success for centering errors of 1.5× the object's radius or less). Among 950 successful grasps of various objects and configurations, the gripper failed to release the object \sim 10 times. This occurred primarily in scenarios with the lightest objects and was resolved by actuating and releasing the gripper a second time. Elements affecting the release of objects are discussed further in SI Appendix, SI Text. Overall, we find that our stochastic entanglement strategy works well for grasping topologically and geometrically complex objects, but is less successful with simpler objects like spheres, cylinders, and cubes, which can be easily grasped by using traditional rigid grippers (12, 13).

The design space of active entanglement can be understood in terms of dimensional analysis. For a single filament of external radius r, internal radius expressed as a fraction (δ) of the external radius δr , $\delta \in [0, 1]$, length l, channel eccentricity ϵr , $\epsilon \in [0, 1]$, elastic modulus E, in an array with a characteristic spacing d, actuated by a pressure p, the design space of the gripper is spanned by the following dimensionless parameters: gripper filament areal density $\phi_G = r^2/d^2 \ll 1$, a scaled pressure p/E, and, finally, the geometric arrangement of the filaments denoted by a scalar S. Additionally, if we also vary the filament length, internal channel radius, and eccentricity, we can control l/r, δ , and ϵ . (Note that this model assumes the simplification of a circular filament crosssection, where SI Appendix, SI Text explains that the simulation takes into account the major and minor axes measured from the physical filaments.) Finally, moving from terrestrial to aquatic environments provides an additional parameter, l/l_g , where $l_g =$ $(Er^2/\Delta\rho g)^{1/3}$ is a gravitational length, with $\Delta\rho$ being the difference in the density between the filament material and the ambient medium. Here, we will focus primarily on varying the gripper areal density of the filaments, ϕ_G , for simplicity, recognizing that there is a vast range of possibilities for future exploration. An object to be grasped, on the other hand, can be characterized by its size, R_T , the topological complexity of its branching structure, which we capture in a simplified form using its effective volumetric density, ϕ_T , within a convex hull around the object and, finally, its mass density, ρ_T , which determines the object weight $\rho_T R_T^3 g$. The efficacy of the gripper is a function of its topological and geometrical complexity, as well as that of the target, and is a function of these dimensionless parameters.

Upon activation, the characteristic curvature, κ , of a filament subject to pressure p scales as $\kappa \sim p(1-\delta)^2 \epsilon/rE$ and follows from a simple torque balance (see SI Appendix, SI Text for details). For grasping when gravitational effects can be neglected (e.g., in an aquatic environment, or when $l/l_g\ll 1$), the radius of curvature of a filament $R\sim \kappa^{-1}$ must be smaller than the overall size of the target R_T , and, furthermore, the length of the filament l must satisfy $l \ge R_T$ to enable distributed contact. This is a conservative estimate, since in an array of filaments of areal density ϕ_G , it may be possible to collectively entangle with the target since the effective curvature of a tangle will scale as $\kappa f(\phi_G)$, where $f(\phi_G) \ge 1$ is a function that depends on the details of the filament-array geometry. Therefore, a simple scaling relation for entanglement grasping via an array of long actuated filaments is given by $pR_T(1-\delta)^2 \epsilon f(\phi_G)/rE \ge 1$. In terrestrial environments, an additional condition is that the weight of the target must be supported by the entanglement, so that $\rho_T R_T^4 g \leq E r^3 p (1 - \delta)^2 \epsilon f(\phi_G)$, a scaling result that follows from the balance between elastic and gravitational torques. These two scaling estimates characterize the geometric and mechanical requirements for grasping. To explore these ideas, we tested filament spatial density by varying the filament spacing (Fig. 3D), object spatial density by varying the branch length of the eightbranch tree (Fig. 3E), and relative density of the object to the filaments by varying test tree mass (Fig. 3F). As expected, we saw a drop in performance when the spatial density of the filaments or target branch length decreased, reducing the probability of entanglement. The largest tree branches also showed a decrease in robustness to normalized centering error, likely due to a combination of increasing mass, a greater offset between contact points and the center of mass, and effectively few accessible branches as the circumferential distance between branches.

In the absence of environmental obstacles, the minimum radius of contact of an actuated (curled) filament is the limiting factor for the smallest objects that it can reliably grasp, though it is possible for two filaments to pick up some objects that may be too small for a single filament. Environmental obstacles can also hinder filaments, which must hang down, around, over, or through a target object under the force of gravity. Future studies might explore dynamically swinging the filaments onto an object or using a jet of air to blow them laterally toward an object. The surface below an object can similarly be an obstacle, though the filaments can lift objects without curling under an object, as demonstrated by the filament wrapping around or inside of a vertical tube (shown in SI Appendix, Fig. S4). Teeple et al. (45) have demonstrated that a soft gripper can pick up fabric from a table. We have accomplished a similar grasp with filaments, but this capability is severely limited by the textile stiffness, surface friction, and normal force. Hawkes et al. (46) have demonstrated a growing vine robot that could be combined with an entanglement concept to push under low-profile objects, but a rigid plate or narrow rod sitting on a flat surface would be impossible to pick up if the filaments cannot curl under the object.

To go beyond the scaling ideas above, we use numerical simulations of a director-based Cosserat continuum framework for slender filamentous objects (47, 48) to explore the mechanics of rods capable of bend, twist, stretch, and shear deformation modes, all necessary to follow the geometrically nonlinear deformations of our elastomeric filamentous actuators, including interfilament contact, friction from sliding contact, gravity, and internal viscous dissipation (48). The actuation of the filaments is accomplished by introducing an intrinsic curvature along the length of the filaments at the instant of actuation and assuming that the actuated shape equilibrates rapidly relative to the dynamics of entanglement or contact creation with the target. In a gravitational field, the gripper filaments curl into helical structures and make contact with other filaments and the target, leading to a soft entangled grasp. Although our simulation framework does not account for the effects of static friction or electrostatic forces due to charge build-up in sliding filaments, it is still capable of capturing the qualitative aspects of entanglement-mediated grasping, replicating our experimental observations (for details, see SI Appendix, SI Text). In Fig. 3 B and C, we show the ability of our simulation framework to tangle with and lift a branched structure (the eight-branch tree), remaining successful until the scaled positioning offset is as large as 30% of the target size, a conservative estimate, given that we have not accounted for frictional effects in the simulations. A side-by-side comparison of the experimental and simulated grasps are shown in Fig. 1D (see also Movie S2).

Our simulations also allow us to explore the phase space spanned by the ratio of the target-object spatial density ϕ_T , the filament spatial density ϕ_G , and a ratio of the density of the target object to that of the gripper, shown in Fig. 3G, with each point being the result of seven simulations, shown along with the results of physical testing by varying filament spacing, branch length, and eight-branch tree mass corresponding to Fig. 3 D-F. The contour plots show the success rate (defined by the ability of the gripper to maintain a grasp for 1 min). The simulated phase space shows a slight underestimate of the performance achieved in physical testing, likely because the effects of static friction were not accounted for.

At smaller scales, we expect the role of gravity and inertia to lessen and for surface forces and drag to become more apparent in the behavior of the filaments. We expect that the combination of increased surface forces and decreased gravity could make it more difficult to release objects without additional external forces from fluid flow or stochastic motions from wriggling the filaments. Critical to the entanglement when scaling up or down, however, is that the aspect ratio of the filaments or tentacles remains high. Depending on how grasping forces are also scaled, this might raise an issue of fragility in the filaments. In the case of scaling the filaments up to larger scales, a challenge becomes accounting for the self-weight of the filaments. If the filaments are actuated pneumatically or hydraulically and have a larger diameter, material challenges may arise from the increased hoop stress in the filaments. To mitigate this, the filaments may not need to be scaled uniformly and could also be actuated by alternative mechanisms, such as tendon drives.

Future iterations of the filament gripper can draw inspiration from biology. Taking inspiration from blackworms, the entangling (and disentangling) behavior of an array of filaments can be calibrated by tailoring the stiffness of the filaments, the rate of actuation, and the relative phase of actuation. While we demonstrate the use of entanglement for grasping, recent studies have also shown how blackworms use entanglement for locomotion of a blob toward or away from a stimulus and protection against inhospitable temperatures and toxins (40). Jellyfish and sea anemones can use toxins to immobilize their prey or microscale barbs to help ensnare prey. Instead of releasing their prey, the ultimate objective is digestion (3). Entanglement grasping might be used to mimic this behavior, collecting prey for nutrients, or perhaps to be used as a method of decontaminating water or waste streams. Alternatively, filament grippers might be used to anchor sensing devices to monitor flora and fauna with tendrils, hair, or other structures conducive to entanglement. Tentaculate predators are also capable of nonvisual sensing of, and reacting to, prey (3). Future iterations of this gripper might take cues from tentaculate of predators that rely on nonvisual cues to trigger a closing response that is tailored to specific targets.

The imprecision of stochastic entanglement is both an advantage and a constraint. Entanglement is best suited for lowprecision tasks, such as gently moving topologically complex or delicate objects that do not require subcentimeter precision. Objects could be inanimate or possibly flora and fauna to be moved into a collection box, planter, cage, or a human hand. This work explores a quasistatic approach to object manipulation, using relatively slow movements and descending over objects from directly above, relying on the overall size of the array of filaments and their curling behavior to accommodate centering error between the gripper and the target object. Future work, however, can explore lateral and dynamic approaches, where filaments are swung onto or into an object's space. Swinging the filaments could further reduce the precision required for grasping, but may similarly reduce the precision of release. Given its compliance, however, a gripper made up of filaments might be made to interact with, and conform with, a more precise receptacle after undertaking a particularly dynamic and less precise grasp. Coupled to a rigid arm or support structure, the filaments would be the primary source of error. Elements that affect error of release include the length of the filaments, the offset between the gripper center and the center of mass of the target object in the initial grasp, and the speed and accelerations applied in the movement of the filaments and target object. The stiffness of the entangled mass can also play a role in the precision of release, which is affected by both the array of filaments and their interaction with the geometry of the target

Secure grasping of an object in both animate (human) and inanimate (robotic) settings requires a characterization of the size, shape, mass distribution, and stiffness of the target and suggests crucial roles for perception, planning, and action with feedback. Here, we demonstrate an embodied solution to this problem, relying on the active entanglement of an array of slender, pneumatically actuated filaments for adaptable grasping without perception, planning, or feedback. Our gripper can entangle, wrap, or cradle target objects via distributed soft contacts and pick up targets with a range of sizes, topological complexities, and geometric shapes. A scaling and computational framework for entangling thin elastic filaments corroborates our experimental observations. All together, our approach to the problem of robotic grasping complements traditional solutions by replacing grippers with few degrees of freedom, but complex feedbackcontrol strategies with infinite-dimensional compliant filaments that are morphologically complex, but operate without feedback. This ability to use complex morphology (geometry and topology) and dynamics (physics) with simple control will expand the range of objects conducive to robotic grasping.

Materials and Methods

The grippers in this work consisted of 12 filaments arranged in a pattern of two concentric circles with a 50-mm and a 25-mm diameter. The filaments were connected to a pneumatic manifold to allow simultaneous external fluidic control of their pressure state. The manifold was printed on an Objet30 polyjet printer in VeroClear rigid resin (Stratasys). The manifold was designed with an interchangeable bracket for mounting directly on a stationary support structure for micro-CT scans, mounting to an Instron material-testing machine, and mounting on a UR5 robot arm. For the micro-CT scans and pull-force testing (on the material testing machine), the filament pressure was manually controlled with a regulator and three-way valve to switch the filaments between their operating pressure and ambient pressure. For the robot-arm grasping tests, a custom pressure controller with solenoid valves was used for automated switching between ambient and operating pressures. The arm position and gripper pressure were both controlled via ROS (Robot Operating System). In all tests, the operating pressure of the filaments was set to 172 kPa. The filaments were fabricated to all operate at the same pressure using dip-coating methods described by Becker et al. (41). More details regarding testing, fluid control, simulations, hardware, and fabrication can be found in SI Appendix, SI Text.

Data, Materials, and Software Availability. Processed data from the micro CT scans, scripts used for entanglement analysis, and experimental data have been made publicly available on GitHub, https://github.com/harvardmicrorobotics/EntanglementGripper (49). The entanglement simulations were created with the open source software, Elastica, which is available at https://www. cosseratrods.org(50) and simulation parameters are listed in the Supplemental

- R. Pfeifer, M. Lungarella, F. Iida, Self-organization, embodiment, and biologically inspired robotics. Science 318, 1088-1093 (2007).
- J. Fleagle, Dynamics of a brachiating siamang (Hylobates (Symphalangus) syndactylus). Nature 248, 259-260 (1974).
- L. P. Madin, Feeding behavior of tentaculate predators: In situ observations and a conceptual model. Bull. Mar. Sci. 43, 413-429 (1988).
- M. T. Mason, Toward robotic manipulation. Annu. Rev. Control. Robot. Auton. Syst. 1, 19.1–19.28
- A. Bicchi, Hands for dexterous manipulation and robust grasping: A difficult road toward simplicity. IEEE Trans. Robot. Autom. 16, 652-662 (2000).
- M. R. Cutkosky, P. K. Wright, Friction, stability and the design of robotic fingers. Int. J. Robot. Res. 5, 20-37 (1986).
- A. Bicchi, On the closure properties of robotic grasping. Int. J. Robot. Res. 14, 319–334 (1995).
- S. Jacobsen, E. Iversen, D. Knutti, R. Johnson, K. Biggers, "Design of the Utah/MIT dextrous hand" in Proceedings: 1986 IEEE International Conference on Robotics and Automation (IEEE, Piscataway, NJ, 1986), Vol. 3, pp. 1520-1532.
- W. Townsend, The BarrettHand grasper-programmably flexible part handling and assembly. Ind. Robot Int. J. 27, 181-188 (2000).
- 10. A. Kochan, Shadow delivers first hand. Ind. Robot Int. J. 32, 15-16 (2005).
- 11. L. B. Bridgwater et al., "The robonaut 2 hand-designed to do work with tools" in 2012 IEEE International Conference on Robotics and Automation (IEEE, Piscataway, NJ, 2012), pp. 3425-3430.
- 12. J. Mahler et al., "Dex-net 2.0: Deep learning to plan robust grasps with synthetic point clouds and analytic grasp metrics" in Proceedings of Robotics: Science and Systems. https://arxiv.org/abs/1703.09312 (8 August 2017).
- 13. D. Morrison, P. Corke, J. Leitner, EGAD! An evolved grasping analysis dataset for diversity and reproducibility in robotic manipulation. IEEE Robot. Autom. Lett. 5, 4368-4375 (2020).
- J. Mahler et al., Learning ambidextrous robot grasping policies. Sci. Robot. 4, eaau4984 (2019).
- O. M. Andrychowicz et al., Learning dexterous in-hand manipulation. Int. J. Robot. Res. 39, 3–20 (2020).
- Y. She et al., Cable manipulation with a tactile-reactive gripper. Int. J. Robot. Res. 40, 1385–1401 (2021).
- N. Kuppuswamy et al., "Soft-bubble grippers for robust and perceptive manipulation" in 2020 IEEE/RSJ International Conference on Intelligent Robots and Systems (IEEE, Piscataway, NJ, 2020), pp.
- 18. L. U. Odhner et al., A compliant, underactuated hand for robust manipulation. Int. J. Robot. Res. 33, 736-752 (2014).
- 19. D. M. Aukes et al., Design and testing of a selectively compliant underactuated hand. Int. J. Robot. Res. 33, 721-735 (2014).
- 20. W. Friedl, H. Höppner, F. Schmidt, M. A. Roa, M. Grebenstein, "CLASH: Compliant low cost antagonistic servo hands" in 2018 IEEE/RSJ International Conference on Intelligent Robots and Systems (IROS) (IEEE, Piscataway, NJ, 2018), pp. 6469-6476.
- 21. M. G. Catalano et al., Adaptive synergies for the design and control of the PISA/IIT SoftHand. Int. J. Robot. Res. 33, 768-782 (2014).
- D. Rus, M. T. Tolley, Design, fabrication and control of soft robots. Nature 521, 467-475 (2015).
- P. Paoletti, G. W. Jones, L. Mahadevan, Grasping with a soft glove: Intrinsic impedance control in pneumatic actuators. J. R. Soc. Interface 14, 20160867 (2017).
- J. Shintake, V. Cacucciolo, D. Floreano, H. Shea, Soft robotic grippers. Adv. Mater. 30, e1707035 (2018).
- R. Deimel, O. Brock, A novel type of compliant and underactuated robotic hand for dexterous grasping. Int. J. Robot. Res. 35, 161-185 (2016).
- J. Zhou, J. Yi, X. Chen, Z. Liu, Z. Wang, BCL-13: A 13-DOF soft robotic hand for dexterous grasping and in-hand manipulation. IEEE Robot. Autom. Lett. 3, 3379-3386 (2018).

ACKNOWLEDGMENTS. This work was supported by Office of Naval Research Grant N00014-17-1- 2063; NSF Grants EFRI-1830901, DMR-1922321, DMR-2011754, DBI-1556164, and EFMA-1830901; NSF Graduate Research Fellowship Grants DGE1144152 and DGE1745303; National Research Foundation of Korea Grant 2021R1A6A3A03039239; the Wyss Institute for Biologically Inspired Engineering; the Simons Foundation; and the Henri Seydoux Fund.

- 27. A. Bhatt, A. Sieler, S. Puhlmann, O. Brock, "Surprisingly Robust In-Hand Manipulation: An Empirical Study" in Proceedings of Robotics: Science and Systems. (27 January 2022). https://doi.org/10.15607/RSS.2021.XVII.089.
- E. Brown et al., Universal robotic gripper based on the jamming of granular material. Proc. Natl. Acad. Sci. U.S.A. 107, 18809-18814 (2010).
- A. Firouzeh, J. Paik, Grasp mode and compliance control of an underactuated origami gripper using adjustable stiffness joints. IEEE/ASME Trans. Mechatron. 22, 2165-2173 (2017).
- S. Li et al., "A vacuum-driven origami "magic-ball" soft gripper" in 2019 International Conference on Robotics and Automation (ICRA) (IEEE, Piscataway, NJ, 2019), pp. 7401-7408.
- 31. W. McMahan et al., "Field trials and testing of the octarm continuum manipulator" in 2006 IEEE International Conference on Robotics and Automation (IEEE, Piscataway, NJ, 2006), pp. 2336–2341.
- 32. R. V. Martinez et al., Robotic tentacles with three-dimensional mobility based on flexible elastomers. Adv. Mater. 25, 205-212 (2013).
- J. Paek, I. Cho, J. Kim, Microrobotic tentacles with spiral bending capability based on shape-engineered elastomeric microtubes. Sci. Rep. 5, 10768 (2015).
- Z. Xie et al., Octopus arm-inspired tapered soft actuators with suckers for improved grasping. Soft Robot. 7, 639-648 (2020).
- B. Mazzolai, L. Margheri, M. Cianchetti, P. Dario, C. Laschi, Soft-robotic arm inspired by the octopus: II. From artificial requirements to innovative technological solutions. Bioinspir. Biomim. 7, 025005 (2012).
- 36. G. Giordano, M. Carlotti, B. Mazzolai, A perspective on cephalopods mimicry and bioinspired technologies toward proprioceptive autonomous soft robots. Adv. Mater. Technol. 6, 2100437 (2021).
- B. Liao et al., Soft rod-climbing robot inspired by winding locomotion of snake. Soft Robot. 7, 500-511 (2020).
- I. Must, E. Sinibaldi, B. Mazzolai, A variable-stiffness tendril-like soft robot based on reversible osmotic actuation. Nat. Commun. 10, 344 (2019).
- S. J. Gerbode, J. R. Puzey, A. G. McCormick, L. Mahadevan, How the cucumber tendril coils and overwinds. Science 337, 1087-1091 (2012).
- Y. Ozkan-Aydin, D. I. Goldman, M. S. Bhamla, Collective dynamics in entangled worm and robot blobs. Proc. Natl. Acad. Sci. U.S.A. 118, e2010542118 (2021).
- K. P. Becker, Y. Chen, R. J. Wood, Soft actuator arrays: Mechanically programmable dip molding of high aspect ratio soft actuator arrays. Adv. Funct. Mater. 30, 2070075 (2020).
- T. J. Jones, E. Jambon-Puillet, J. Marthelot, P. T. Brun, Bubble casting soft robotics. Nature 599,
- 43. G. Buck, J. Simon, The spectrum of filament entanglement complexity and an entanglement phase transition. Proc.- Royal Soc., Math. Phys. Eng. Sci. 468, 4024-4040 (2012).
- 44. D. J. Montana, Contact stability for two-fingered grasps. IEEE Trans. Robot. Autom. 8, 421-430 (1992).
- C. B. Teeple, T. N. Koutros, M. A. Graule, R. J. Wood, Multi-segment soft robotic fingers enable robust precision grasping. Int. J. Robot. Res. 39, 1647-1667 (2020).
- E. W. Hawkes, L. H. Blumenschein, J. D. Greer, A. M. Okamura, A soft robot that navigates its environment through growth. Sci. Robot. 2, eaan 3028 (2017).
- 47. E Cosserat, F Cosserat, Théorie des Corps Déformables (A. Hermann et fils,), (Hermann, Paris, France,
- M. Gazzola, L. H. Dudte, A. G. McCormick, L. Mahadevan, Forward and inverse problems in the mechanics of soft filaments. R. Soc. Open Sci. 5, 171628 (2018).
- K. Becker et al., harvard-microrobotics/EntanglementGripper. GitHub. https://github.com/harvardmicrorobotics/EntanglementGripper. Deposited 26 September 2022.
- Gazzola Lab, University of Illinois at Urbana-Champaign, Elastica: An open-source software package for simulating assemblies of Cosserat rods. Elastica. https://www.cosseratrods.org. Accessed 29 September 2022.